IMMUNOLOGY

Graphene quantum dots as anti-inflammatory therapy for colitis

Byung-Chul Lee[1]*[†], Jin Young Lee[1]*[‡], Juhee Kim[2], Je Min Yoo[2§], Insung Kang[1], Jae-Jun Kim[1], Nari Shin[1], Dong Jin Kim[3], Soon Won Choi[1], Donghoon Kim[4], Byung Hee Hong[2,4,5||], Kyung-Sun Kang[1||]

While graphene and its derivatives have been suggested as a potential nanomedicine in several biomimetic models, their specific roles in immunological disorders still remain elusive. Graphene quantum dots (GQDs) may be suitable for treating intestinal bowel diseases (IBDs) because of their low toxicity in vivo and ease of clearance. Here, GQDs are intraperitoneally injected to dextran sulfate sodium (DSS)–induced chronic and acute colitis model, and its efficacy has been confirmed. In particular, GQDs effectively prevent tissue degeneration and ameliorate intestinal inflammation by inhibiting T_H1/T_H17 polarization. Moreover, GQDs switch the polarization of macrophages from classically activated M1 to M2 and enhance intestinal infiltration of regulatory T cells (T_{regs}). Therefore, GQDs effectively attenuate excessive inflammation by regulating immune cells, indicating that they can be used as promising alternative therapeutic agents for the treatment of autoimmune disorders, including IBDs.

INTRODUCTION

Intestinal bowel diseases (IBDs) including Crohn's disease and ulcerative colitis are destructive, relapsing tissue disorders that involve dysregulation of the local immune response and compromised intestinal barrier function (1). The pathophysiology of IBDs is associated with exaggerated T cell responses (2) and related macrophages, which are one of the most abundant myeloid cells in the peritoneal cavity, including intestinal mucosa. The extensive interactions between T cells and macrophages deteriorate inflammation. Therefore, understanding the mechanism of macrophage's regulation on T cell differentiation is essential in developing previously unidentified therapeutics for IBDs. Many approaches have been made to find a way to cure IBDs, and alternative therapeutics are in urgent need as the disease prevails throughout the world (3). Although the use of immunosuppressive drugs is one of the main treatments (4) and methods to increase the drug delivery to lesion have also been developed (5), the treatments for IBDs are often accompanied by complications such as infections and malignancies (6). Thus, alternative drug with less side effects is still needed. Recent studies have suggested suitable mouse models for Crohn's disease by introducing genetic modifications and particular microorganisms (7). Nevertheless, impaired intestinal barrier function and subsequent dysregulated immune response are still considered as a crucial factor for disease onset (1). To address this issue, we tried graphene quantum dots (GQDs) as therapeutics in colitis model mice because previous research has shown that graphene derivatives interact with immune cells including macrophages and T cells (8).

Graphene derivatives, especially GQDs, have high biocompatibility and antioxidant effect, so GQDs have been exploited as a potential therapeutic agent for treating inflammatory diseases (9). GQDs can scavenge reactive oxygen radicals by delocalizing electron density in the conjugated ring structure; hence, they are able to reduce oxidative stress. Besides, there are abundant anionic functional groups on the edges, in which the property is known to provoke fewer immune responses compared to positively charged nanoparticles (10). In addition, previous studies showed the potential uses of graphene materials in vaccines, immunotherapeutics, and immunosuppressive agents (11). However, there are few reports on graphene material's roles in autoimmune diseases including IBDs.

IBDs have frequently been studied using the dextran sulfate sodium (DSS) colitis animal model due to its simplicity, reproducibility, and rapidity (12). Notably, the clinical and histological features of DSS-induced animals are very similar to those observed in human patients. DSS disrupts colonic epithelium, leading to the entry of luminal bacteria and antigens into the mucosa and resulting in stimulation of immune cells and secretion of proinflammatory cytokines and chemokines (13). Furthermore, a polarized T helper 1 (T_H1) response and proinflammatory macrophages have been reported to aggravate the inflammatory response in DSS colitis model. For these reasons, we used the DSS colitis model to identify the inhibitory effects of GQDs on acute and chronic colitis.

Our previous study showed that GQDs have protective effects on Parkinson's disease by direct interaction with α-synuclein fibrils without toxicity and can be excreted by urine (14). In this study, we also confirmed the therapeutic effects of GQDs on colitis model mice without any complications. The ex vivo and in vitro analyses were proceeded to investigate the underlying mechanisms of the therapeutic effects of GQDs, which regulated T cell and macrophage subsets to facilitate the disease recovery.

[1]Adult Stem Cell Research Center and Research Institute for Veterinary Science, College of Veterinary Medicine, Seoul National University, Seoul 08826, Republic of Korea. [2]Department of Chemistry, College of Natural Sciences, Seoul National University, Seoul 08826, Republic of Korea. [3]Program in Nano Science and Technology, Graduate School of Convergence Science and Technology, Seoul National University, Seoul 08826, Republic of Korea. [4]Biographene Inc., Advanced Institute of Convergence Technology, Suwon 16229, Republic of Korea. [5]Graphene Research Center, Advanced Institute of Convergence Technology, Seoul National University, Suwon 16229, Republic of Korea.
*These authors contributed equally to this work.
†Present address: Translational Stem Cell Biology Branch, National Heart, Lung, and Blood Institute, National Institutes of Health, Bethesda, MD 20892, USA.
‡Present address: Department of Medicine, Cardiovascular Research Institute, UCSF, San Francisco, CA 94143, USA.
§Present address: Biographene Inc., 555 W 5th St 35th Floor, Los Angeles, CA 90013, USA.
||Corresponding author. Email: kangpub@snu.ac.kr (K.-S.K.); byunghee@snu.ac.kr (B.H.H.)

RESULTS

Characterization of GQDs

GQDs were synthesized by the improved Hummer's method according to the previous literature (fig. S1A) (15). Transmission electron

microscopy (TEM) image showed the lateral size distribution of the GQDs, which had an average size of 28.5 ± 9.7 nm (fig. S1B). The height of the synthesized GQDs was determined by atomic force microscopy (AFM), which showed 7.1 ± 1.8 nm (fig. S1C). The properties of GQDs were further determined by Raman spectroscopy (fig. S1D), exhibiting distinctive D and G bands at 1360 and 1600 cm^{-1}, which are the characteristic peaks of graphene-based materials. GQDs displayed intense and broad D band, which arose from the presence of many defect sites. Functional groups of GQDs were verified by Fourier-transform infrared spectroscopy (FT-IR), elemental analysis (EA), and x-ray photoelectron spectroscopy (XPS). The major peaks from the FT-IR (fig. S1E) spectrum of GQDs were O—H (3430 cm^{-1}), C═O (1730 cm^{-1}), C═C (1620 cm^{-1}), and C—O (1220 cm^{-1}), showing the presence of hydroxyl, carboxyl groups, and epoxide rings. Successful coupling of biotin was proved by the appearance of new peaks at 1400 cm^{-1} (C—H) and at 1080 cm^{-1} (C—O), both derived from polyethylene glycol (PEG). More intense transmittance was observed around 3420 and 1610 cm^{-1} due to the newly formed amide bond. The ratio of oxygen to carbon of GQDs was measured by EA (table S1), and the value 0.73 showed the highly oxidized state of graphite. Through XPS (fig. S1F), the binding energy of C—C (284.50 eV), C—O (286.68 eV), and C═O (288.36 eV) bonds was measured. The C—C bond showed the highest content of 50.54%, and the percentage of C—O and C═O was 38.21 and 11.25%, respectively. The surface charge of GQDs was evaluated by zeta potential, in which the measured value −52.2 ± 6.85 mV showed a highly negatively charged surface and well-dispersed property. On the basis of the measured properties of GQDs, we sought to explore the impact of its therapeutic effects against DSS-induced mice.

GQDs ameliorate DSS-induced colitis in mice

To investigate the therapeutic efficacy of GQDs against IBDs, we established chronic and acute colitis models using DSS (Figs. 1A and 2A). DSS-induced colitis mice were intraperitoneally injected with GQDs after the induction of colitis, and the body weight, survival rate, and disease activity of the mice were monitored. The treatment of GQDs increased survival rates (Fig. 2B) and reduced loss of body weight (Figs. 1B and 2C) in both models, suggesting a probability of the amelioration of the disease. Consistent with the results, the disease activity index (DAI) values were significantly decreased in the presence of GQDs (Figs. 1C and 2D). The shortening of the colon, which is the characteristic pathological feature of colitis, was substantially inhibited as well (Figs. 1D and 2E). Myeloperoxidase (MPO) level, a commonly used biomarker of colitis, is a neutrophil granule constituent, where its level is proportional to the number of migrated neutrophils. In the GQD-treated group, the MPO activity in colon tissues decreased by 45% compared to the phosphate-buffered saline (PBS)–treated mice, implying that GQDs suppressed the infiltration of neutrophils (Fig. 2F). Histological analysis also showed the inhibitory effect of GQDs on colonic inflammation, which exhibited retainment of the intestinal epithelium and less infiltration of immune cells. From picrosirius red and Masson's trichrome staining, the generation of fibrotic tissues was reduced in both models (Figs. 1E and 2G). The secretion of interferon-γ (IFN-γ), the major cytokine involved in IBDs, was markedly reduced in the GQD-treated mice (Figs. 1F and 2H). Besides, in the presence of GQDs, the level of other proinflammatory cytokines—tumor necrosis factor–α (TNF-α), interleukin-6 (IL-6), and MCP-1—was also decreased. Collectively, GQDs showed preventive and therapeutic effects in both acute and chronic colitis models.

GQDs do not exert toxic effects on general health and are naturally excreted

After the sacrifice of colitis-induced mice, we observed an accumulation of GQDs in the abdominal cavity, particularly on greater omentum and mesentery near spleen and colon (fig. S2). To assess the toxicity and excretion of GQDs, we monitored the general health conditions of the mice until 16 weeks from GQD injection. The body weights, as well as the consumption of water and food, were not significantly different compared to those of the control group (Fig. 3, A and B). Also, a negligible difference was found between the weights of organs (Fig. 3C).
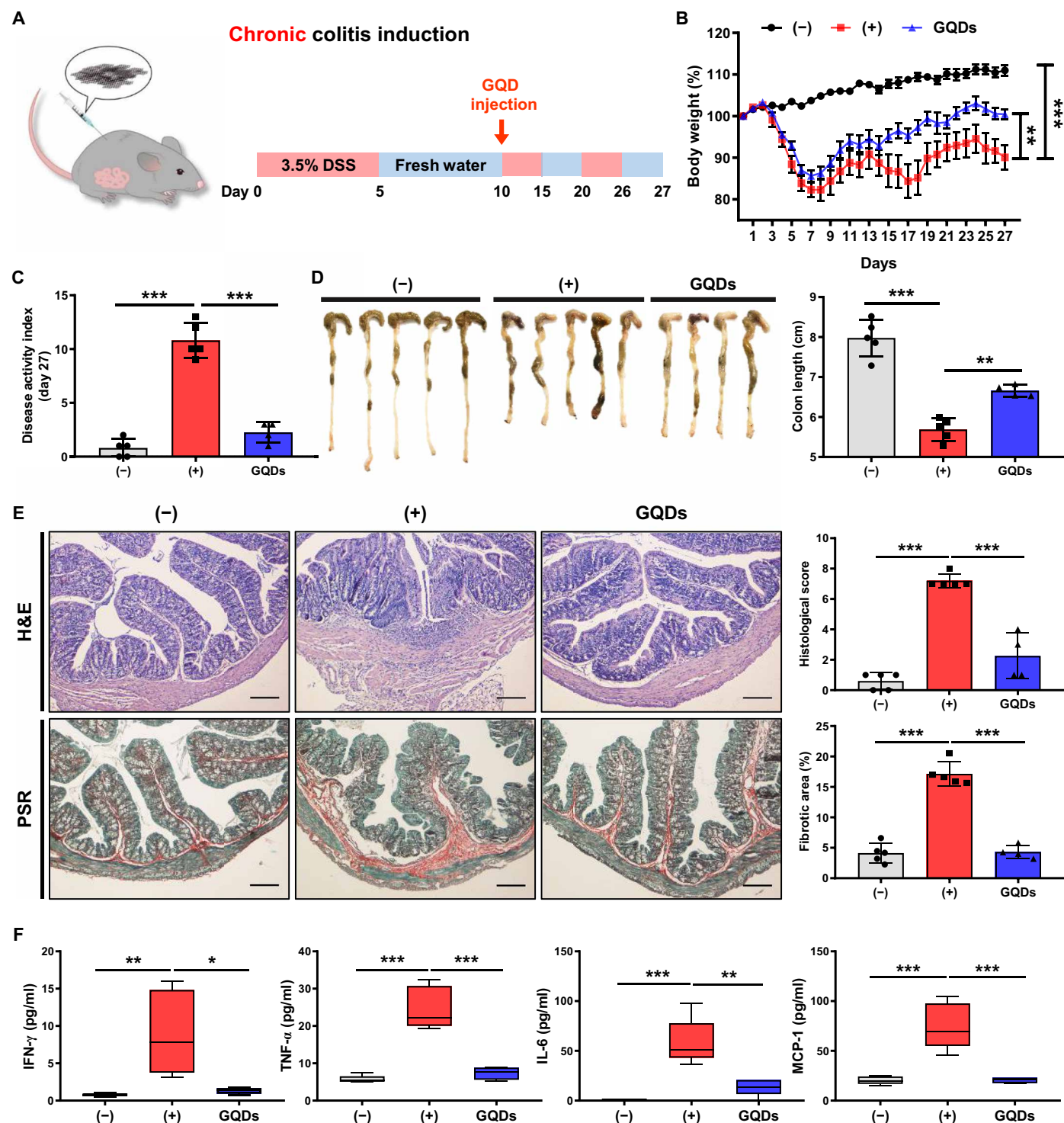
To determine whether GQDs could affect the immune system, proportions of immune cells in the spleen were assessed. GQDs did not change the immune cell proportions (fig. S3), and dysregulated immune reaction did not occur until 16 weeks based on the level of inflammatory cytokines measured (fig. S4). The concentration of IL-6, MCP-1, and TNF-α in serum immediately increased at 2 hours after the injection. However, the levels of these cytokines were stabilized by day 1, and similar levels were maintained with the control group.

In addition to the general health status of the mice, we injected biotin-labeled GQDs and assessed its fate using a fluorescein isothiocyanate (FITC)–conjugated anti-biotin antibody. Notably, the fluorescence in the abdominal mesentery gradually decreased with time, suggesting excretion of biotin-labeled GQDs (Fig. 3D). Moreover, as we reported in a previous article (14), intraperitoneally injected GQDs were cleared out through urine despite their relatively larger size (Fig. 3E). A gradual decrease in the GQD concentration was observed over time, implying a successful excretion. Therefore, we concluded that the dosage and injection methods we used in the colitis model did not cause severe toxicity or disruption in the immune system in mice and that GQDs could be excreted out of the body.

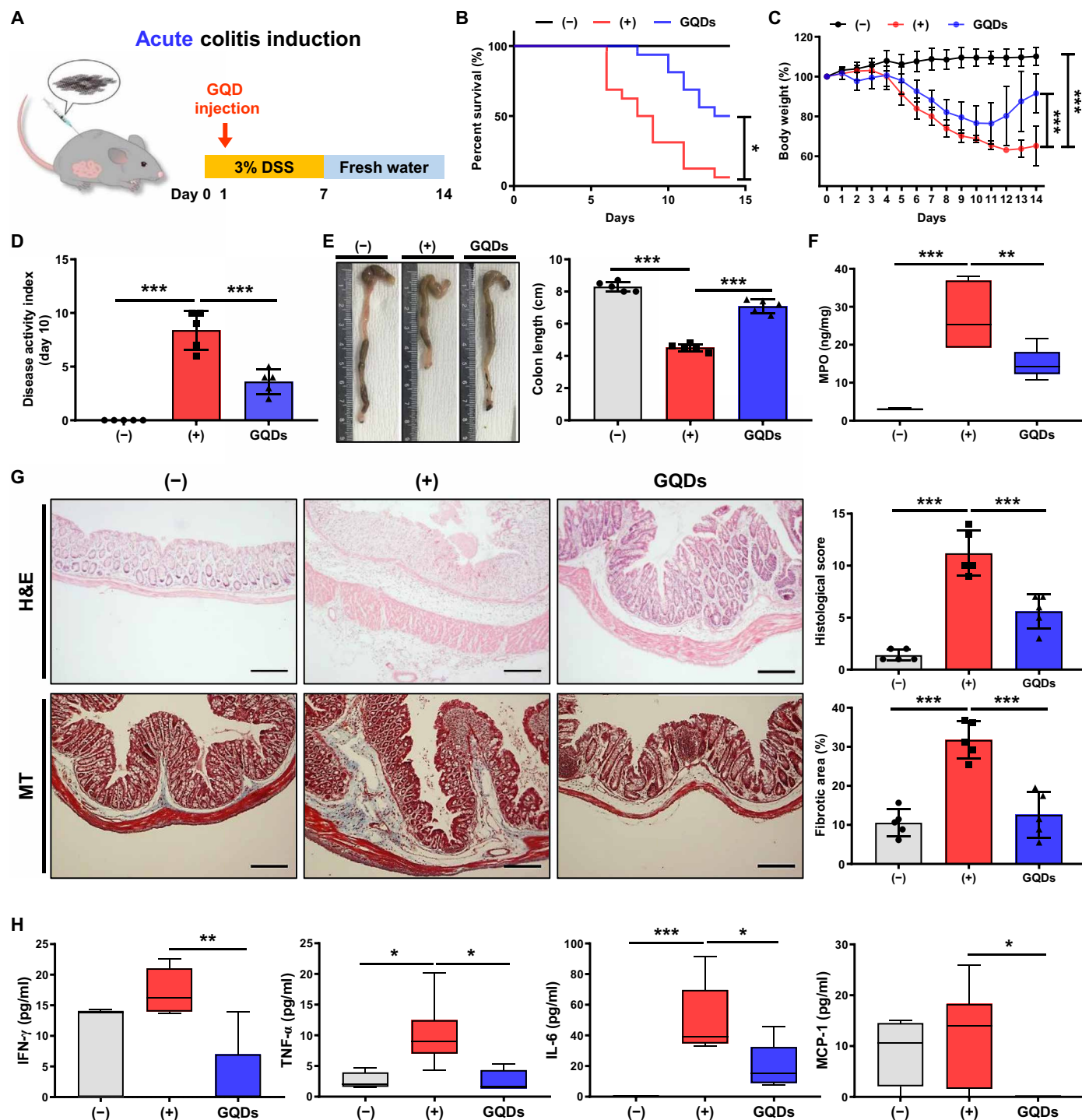## GQDs potently inhibit the development of T$_H$1 cells

The administration of GQDs to the DSS-induced colitis model inhibited the swelling of spleens (fig. S5A). Therefore, we sought to perform a set of ex vivo and in vitro analyses to discriminate the influences of GQDs on cells of the innate and adaptive immune systems. As T$_H$1 cells secrete the major proinflammatory cytokine, IFN-γ, and play a crucial role in intestinal inflammation, we assessed the direct effect of GQDs on CD4$^+$ T cells. GQDs decreased the number of T$_H$1 cells in the spleen of the DSS-induced colitis model (Fig. 4A). IL-12, which promotes the differentiation of CD4$^+$ T cells into T$_H$1 cells, was reduced as well, inhibiting the differentiation toward T$_H$1 cells (Fig. 4B).

To assess the direct effects of GQDs on T cells, human umbilical cord blood (hUCB)–derived CD4$^+$ T cells were treated with various concentrations of GQDs to determine the optimal concentration, where GQDs (20 μg/ml) effectively suppressed the proliferation of T cells (6 to 70%). Notably, GQDs contained the proliferation of primary CD4$^+$ T cells and primary splenocytes (Fig. 4C and fig. S5B). Although no significant influence on the apoptotic pathway was observed, GQDs managed to slightly increase the number of cells in the G$_1$ cell cycle stage, suggesting a suppressed cell cycle progression (fig. S5, C and D). To investigate the direct effects of GQDs on T$_H$1 polarization, isolated naïve CD4$^+$ T cells were differentiated into the T$_H$1 cells in the presence of GQDs. GQDs reduced T$_H$1 differentiation (Fig. 4, D and E), and consistent results were found in the gene expression pattern (Fig. 4F). To analyze functional changes in GQD-treated T$_H$1 cells, we measured the concentration of cytokines
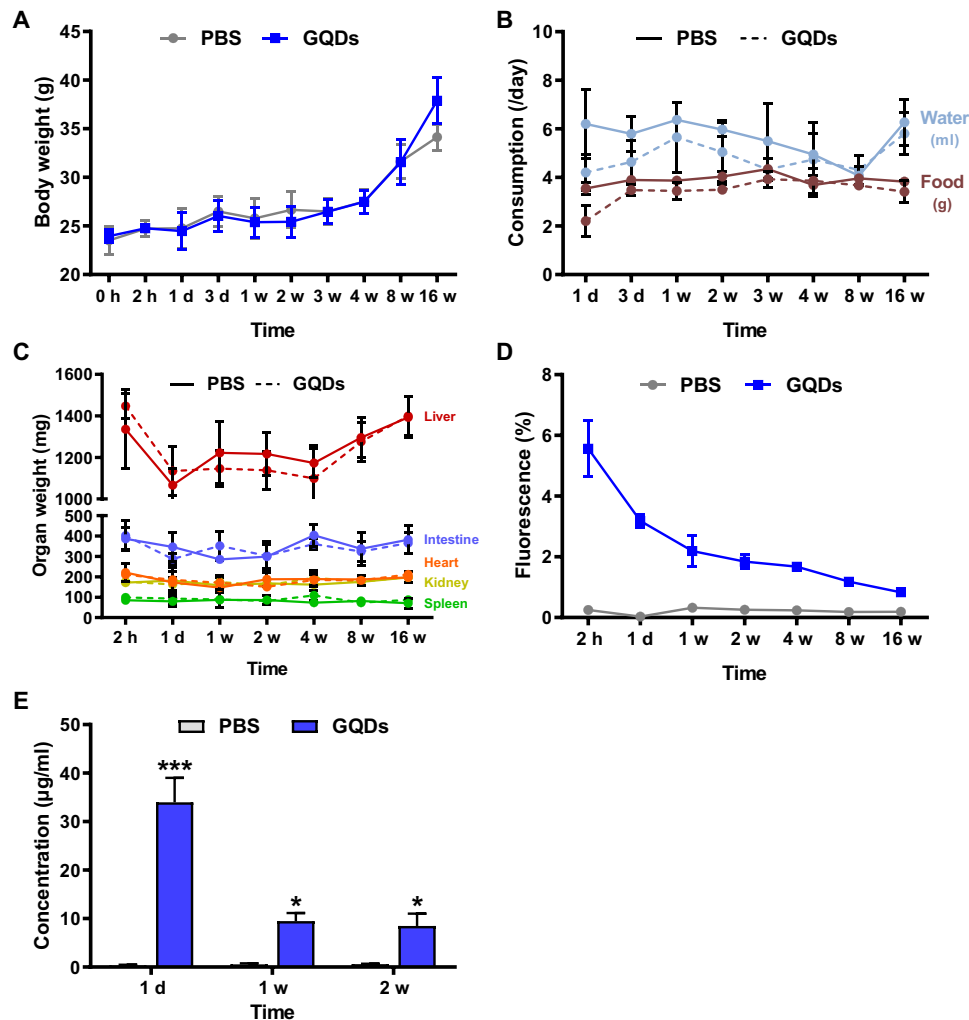
Fig. 1. Intraperitoneal injection of GQDs effectively alleviates DSS-induced chronic colitis in mice. (**A**) Experimental scheme for DSS-induced chronic colitis and GQD administration. DSS water (3.5%) was repetitively administered to mice to induce colitis. GQDs were injected intraperitoneally (300 μg per head) 10 days after the administration of DSS. (**B** to **F**) Mice received intraperitoneal injection of GQDs after chronic DSS colitis induction. On day 27, mice were sacrificed for further investigation. (B) The percentage of body weight change and (C) the DAI for colitis severity were monitored for clinical assessment. (D) After 27 days from colitis induction, the lengths of the colons obtained from each group were measured. Photo credit: Byung-Chul Lee (Adult Stem Cell Research Center and Research Institute for Veterinary Science, College of Veterinary Medicine, Seoul National University). (E) Left: Representative images of colon sections stained with hematoxylin and eosin (H&E) and picrosirius red (PSR) staining for the assessment of histology and fibrosis. Scale bar, 200 μm. Right: Histopathologic evaluations were conducted to examine lymphocyte infiltration and intestinal damage. Quantitative analysis of the fibrotic area (stained in red). (F) Serum was collected from the colitis mice, and the secreted levels of the indicated cytokines were assessed using CBA analysis. $N = 4$ to 5 mice per group. *$P < 0.05$, **$P < 0.01$, and ***$P < 0.001$. Results are shown as means ± SD.

Fig. 2. Intraperitoneal injection of GQDs suppresses DSS-induced acute colitis in mice. (**A**) Experimental scheme for acute colitis induction using DSS and administration of GQDs. (**B** to **H**) Mice received intraperitoneal injection of GQDs after acute DSS colitis induction. On day 14, mice were sacrificed for further investigation. (B) The survival rate and (C) percentage of body weight change were monitored for clinical assessment of colitis severity ($N = 14$ to 16 mice per group). (D) The DAI on day 10 were monitored. (E) Mice were sacrificed 14 days after the induction of colitis with DSS, and colon lengths were measured to determine intestinal damage. Photo credit: Byung-Chul Lee (Adult Stem Cell Research Center and Research Institute for Veterinary Science, College of Veterinary Medicine, Seoul National University). (F) The MPO level in the colon tissues was measured. (G) Left: Representative images of colon sections stained with H&E and Masson's trichrome (MT) staining for the assessment of fibrosis. Scale bar, 200 μm. Right: Histopathologic evaluations were conducted to assess lymphocyte infiltration and intestinal damage. Quantitative analysis of fibrotic area (stained in blue). (H) Serum was collected from the colitis mice, and the secreted levels of the indicated cytokines were assessed using CBA analysis ($N = 5$ mice per group). *$P < 0.05$, **$P < 0.01$, and ***$P < 0.001$. Results are shown as means ± SD.

Fig. 3. GQDs are excreted from mice without generating toxicity. Without DSS induction, biotin-labeled GQDs were injected into normal mice by the same method and dosage, and monitored for 16 weeks ($N = 5$ mice per group). (**A**) Body weights and (**B**) water and food consumption were measured at each time point. (**C**) Mice were sacrificed at the indicated time points, and organ weights were assessed. (**D**) The FITC-labeled anti-biotin antibody was used to detect the presence of GQDs in the abdominal mesenteric fat. (**E**) Excretion of GQDs was investigated in urine collected from the mice. $*P < 0.05$ and $***P < 0.001$. Results are shown as means ± SD.
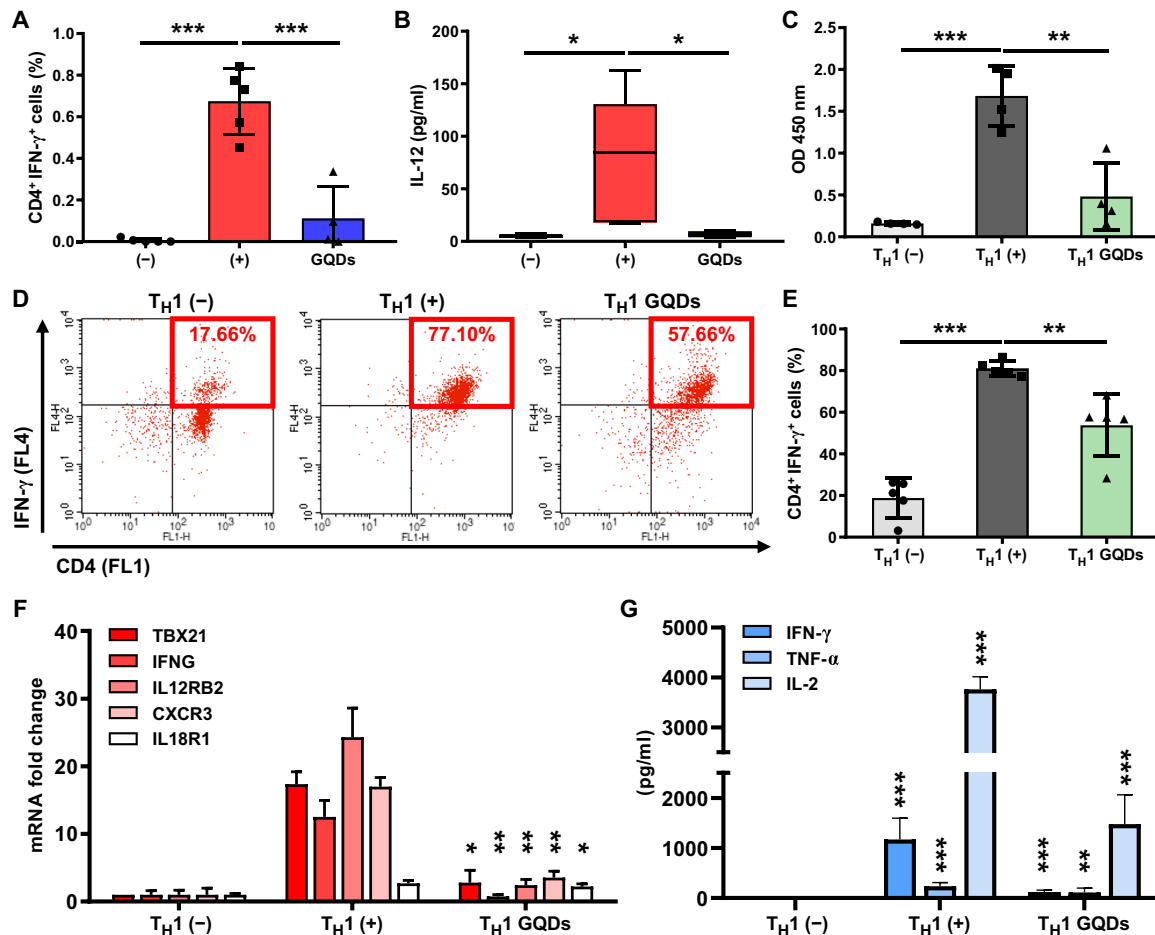
secreted in the cell culture supernatant (Fig. 4G). Proinflammatory cytokines (especially IL-2, IL-12, and IFN-γ) and transcription factor T-bet (TBX21), which have crucial roles in the lineage commitment of T_H1 cells (16), and GQD treatment successfully lowered the cytokine levels and expression of TBX21. Therefore, GQDs alleviate colitis by not only suppressing the proliferation of CD4$^+$ T cells but also restraining T_H1 polarization.

GQDs increase T_{reg} infiltration in vivo

Regulatory T cells (T_{regs}) protect tissues from robust inflammation and facilitate tissue healing by suppressing activated proinflammatory immune cells. Transforming growth factor–β1 (TGF-β1) and IL-10 are major inducers and products of T_{regs} and play crucial roles in T_{reg}-mediated colitis alleviation (17). We (18) and others (19) have previously demonstrated that the activation of T_{regs} accompanied recovery from experimental colitis. In line with this observation, the administration of GQDs increased the splenic polarization (fig. S6A) and colonic infiltration (Fig. 5, A and B, and fig. S6B) of the T_{reg} population.

The secretion of TGF-β1 (Fig. 5C) and IL-10 (Fig. 5D and fig. S6C) was increased by GQD treatment in the DSS-induced colitis model. Again, whether GQDs could directly affect the polarization of T_{regs} was verified. In the presence of GQDs, naïve CD4$^+$ cells were induced toward the T_{reg} lineage. Although GQDs did not increase the polarization of T_{reg} (Fig. 5E), it enhanced the colonic and splenic infiltration of T_{regs} via increased IL-10 and TGF-β1 production.

Moreover, GQDs impeded the colonic infiltration of the mucosal effectors, T_H17 cells (Fig. 5F), and their secretion of IL-17A (Fig. 5G), which have a pivotal role in onset and progression of IBDs (19, 20). The innate immune cell–derived cytokine IL-23, which is a prominent inducer of T_H17 polarization (21), was markedly diminished by GQD treatment (Fig. 5H). As shown in Figs. 1F and 2H, suppression of excessive inflammation was followed by a decrease of proinflammatory cytokines, including IL-6. In the presence of TGF-β1, reduction of IL-6 and IL-23 could inhibit the generation of T_H17 cells and accelerate compensatory T_{reg} development, which leads to a restoration of exaggerated inflammatory responses. Overall, the results

Fig. 4. GQDs suppress T_H1-type immune responses. (**A** and **B**) Colons and serum samples were collected from chronic colitis–induced mice after administration of GQDs ($N = 4$ to 5 mice per group). (A) Proportions of CD4 and IFN-γ–expressing T_H1 cells in the colon were analyzed by flow cytometric analysis. (B) IL-12 secretion levels in the serum were measured by CBA analysis. (**C**) Primary $CD4^+$ T cells were isolated from human cord blood and cultured in the presence of anti-CD3/28 microbeads and GQDs for 2 days, and proliferation was assessed with a BrdU assay. OD, optical density. (**D** to **G**) Human primary $CD4^+$ T cells were induced to differentiate into T_H1 cells using anti-CD3/28 beads in combination with recombinant IL-2, IL-12, and IFN-γ in the presence of GQDs for 5 days. (D and E) The proportion of $CD4^+IFN-γ^+$ cells was determined by flow cytometric analysis. (D) Representative dot plot images. (E) Histogram of collective data. (F) mRNA expression levels in each group of induced T_H1 cells were investigated for the indicated T_H1-specific markers. (G) The indicated T_H1-specific cytokines in the supernatant of T_H1 cells were analyzed by CBA analysis ($n = 4$ to 5). *$P < 0.05$, **$P < 0.01$, and ***$P < 0.001$. Results are shown as means ± SD.

indicate that GQDs increase the infiltration of T_{regs} and restore immune balance in vivo without direct regulation of T_{regs}.
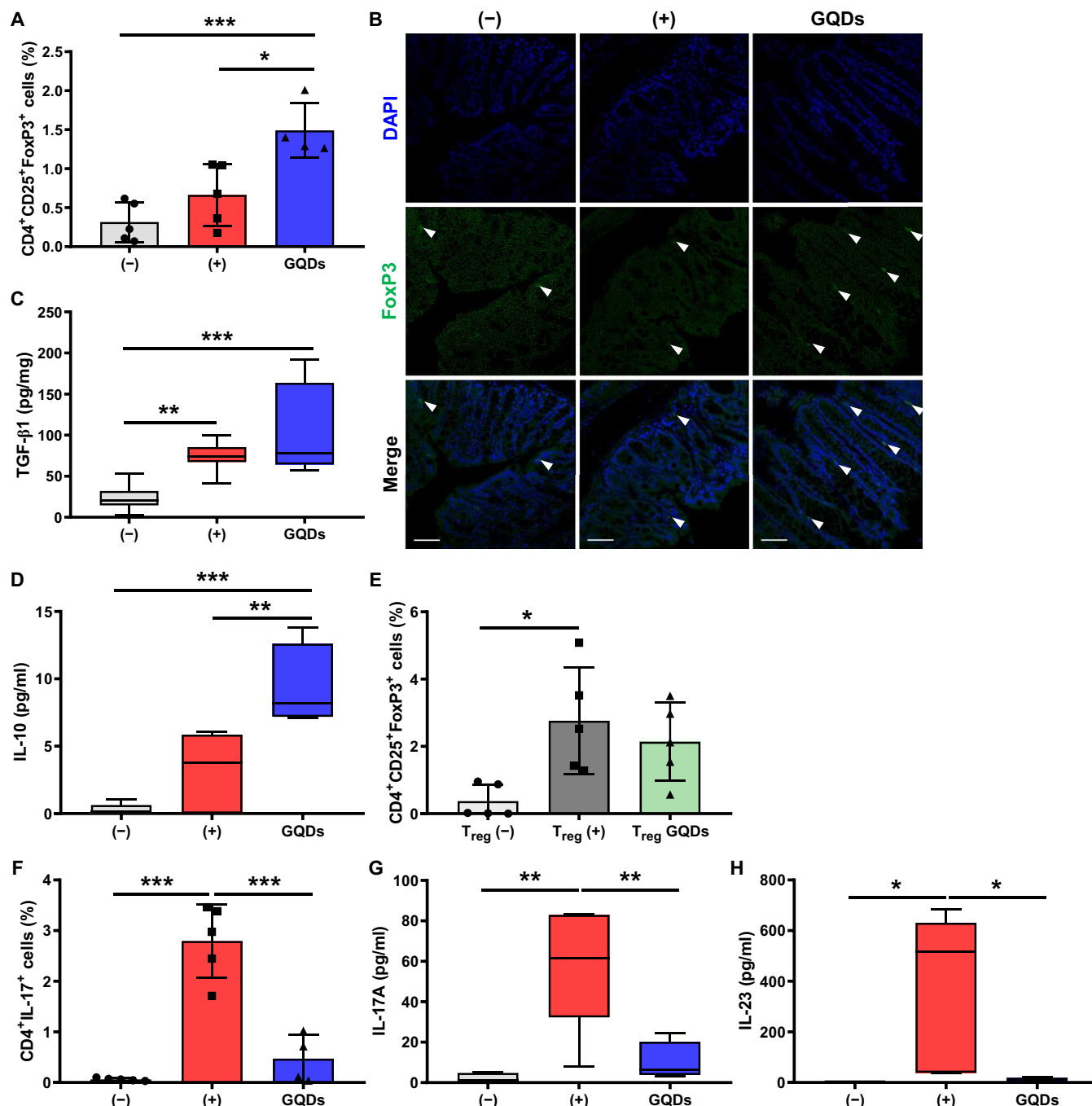
GQDs induce polarization toward M1 macrophages but subsequently convert to M2

Although an imbalance between the tolerogenic and protective immune responses of intestinal macrophages elicits colonic inflammation (22), the symptoms of colitis can be relieved by alternatively activated M2-type macrophages, which have a role in recruiting T_{regs} and their secreted cytokines (23). Therefore, the effects of GQDs toward type-specific polarization of macrophage were investigated. GQDs induced naïve $CD14^+$ cells to become more classical-type macrophages, M1, without any supplementary cytokines (fig. S7A). When $CD14^+$ cells were induced to polarize to M1 in the presence of GQDs, although expression of CD86 was simultaneously elevated, GQDs managed to increase both the $CD14^+CD206^+$ and $CD14^+CD163^+$ populations in M1-type cells (Fig. 6, A and B). Subsequent secretion of TNF-α and IFN-γ was markedly decreased, indicating a reduced

polarization of M1 macrophages (Fig. 6C). Moreover, GQD treatment suppressed the mRNA levels of proinflammatory cytokines and the M1-specific transcription factor IRF5 (fig. S7B).

In the case of polarization toward M2, the expression of CD206 on M2-type macrophages was decreased in the presence of GQDs (fig. S7A). The level of IL-10, the most prominent marker of M2 macrophages, was increased; however, GQD treatment inhibited the expression of CLEC7A and IL-1ra, which are the genes related to M2a subtype (fig. S7B).

As macrophages are known to regulate differentiation of T cells, GQD-treated macrophages were cocultured with $CD4^+$ T cells. As a result, the GQD-treated macrophages promoted the development of T_{regs} (Fig. 6D). Therefore, GQDs play a role in the resolution of inflammation by down-regulating the M1-like features of macrophages and converting them to anti-inflammatory M2 macrophages. This is possible as macrophages display distinctive plasticity and the ability to modify their properties in response to environmental stimuli.
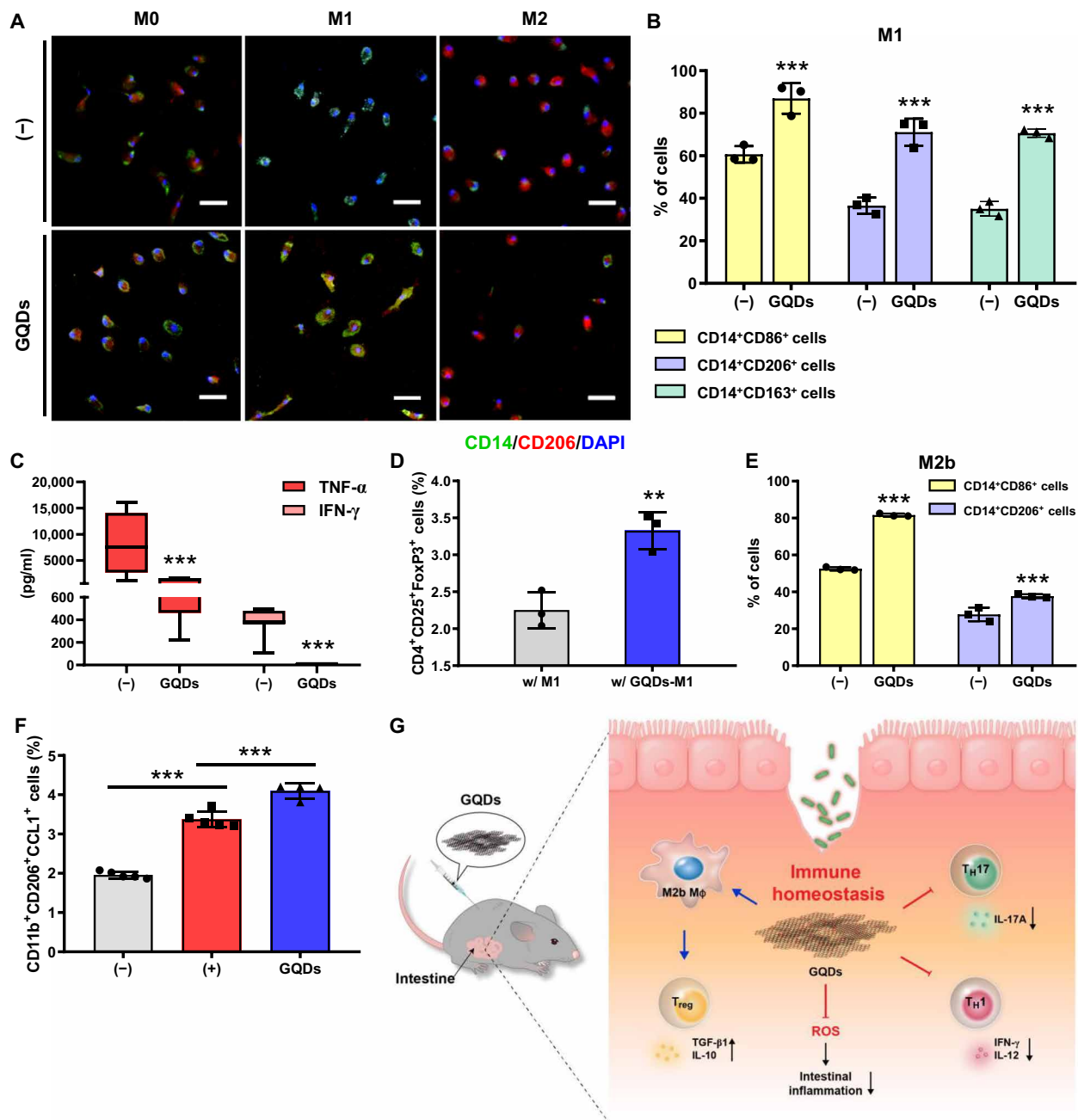
Fig. 5. The effects of GQDs on cell fate decisions of T_{regs} and T_H17 cells. (A, D, and **F** to **H**) The GQD-treated mice with chronic colitis were sacrificed, and colons and serum samples were collected for further ex vivo examination ($N = 4$ to 5 mice per group). (A) Colonic infiltration of CD4$^+$CD25$^+$FoxP3$^+$ T_{regs} was assessed by flow cytometric analysis. (**B** and **C**) The GQD-treated mice with acute colitis were sacrificed, and colons were collected for further ex vivo examination ($N = 8$ to 12 mice per group). DAPI, 4',6-diamidino-2-phenylindole. (B) T_{regs} in the colon were observed by immunostaining of FoxP3 (green). FoxP3$^+$ cells are indicated as arrows. Scale bar, 50 μm. (C) TGF-β1 expression in the colons was detected by ELISA. (D) IL-10 level was determined by CBA analysis. (**E**) CD4$^+$ T cells were isolated from human cord blood, polarized into T_{regs} with specific cytokines, and the proportions of CD4$^+$CD25$^+$FoxP3$^+$ cells were determined by flow cytometric analysis ($n = 5$). (F) Proportions of T_H17 cells in the spleens were analyzed. The indicated T_H17-specific cytokines, (G) IL-17A, and (H) IL-23 in the serum were analyzed. *$P < 0.05$, **$P < 0.01$, and ***$P < 0.001$. Results are shown as means ± SD.

GQDs specifically promote polarization of M2b subtype, leading to the increased infiltration of T_{regs}

Given that the infiltration of colonic T_{regs} was increased and that M2-converted macrophage promoted the development of T_{regs} (Fig. 6D), GQDs have a potential role in the formation of a reciprocal regula-tory loop of T_{regs} and intestinal macrophages via IL-10 and TGF-β1 signaling.

M2 macrophages are categorized into at least three different pop-ulations that have distinct cellular characteristics, gene profiles, and functions, which are mediated by the production of several cytokines

Fig. 6. GQDs promote M2 polarization of macrophages. (A and **B)** Primary CD14^{+} macrophage-like cells were polarized into M1-type cells. (A) CD14^{+} macrophage-like cells were isolated from human cord blood and polarized into M0-, M1-, and M2-type cells with specific inducer cytokines in the presence of GQDs. The cells were immunostained for the cell surface markers CD14 and CD206. Scale bar, 50 μm. (B) M1-polarized macrophages were analyzed by the type-specific cell surface CD markers CD86, CD206, and CD163 using flow cytometry. (**C**) The indicated cytokine concentrations were measured in supernatants of M1 macrophages. (**D**) M1-induced cells in the presence of GQDs were cocultured with naïve CD4^{+} T cells supplemented with IL-2 and TGF-β1, and the proportions of T$_{regs}$ were investigated by flow cytometry. (**E**) In vitro M2b polarization was analyzed by flow cytometric analysis ($n = 3$). (**F**) The presence of M2b macrophages in the peritoneum of chronic colitis–induced mice was detected by flow cytometric analysis ($N = 4$ to 5 mice per group). (**G**) Schematic diagram for the present study. **$P < 0.01$ and ***$P < 0.001$. Results are shown as means ± SD.

(*24*). Among these cells, M2a and M2b macrophages appear to exhibit immunoregulatory activities, while M2c macrophages are responsible for immunosuppressive activities and tissue remodeling (*25*). Interactions between the macrophage subtypes and graphene derivatives have not been previously elucidated. As IL-10 expression was increased, whereas the M2a markers CLEC7A and IL-1ra

were reduced (fig. S7B), GQDs could up-regulate specific subtypes of M2 macrophages. To address the issue, we differentiated naïve CD14^{+} cells into M2a, M2b, and M2c macrophages in the presence of GQDs. The expression of CD206 and CD163 on M2a macrophages was markedly reduced, while there was no notable change in M2c subtype cells (fig. S7C). Notably, the expression of CD86 and

CD206 on macrophages in M2b polarizing conditions was elevated (Fig. 6E). Coherently, the proportion of M2b-subtype macrophages was increased by GQD treatment in DSS-induced mice (Fig. 6F). Therefore, GQDs decreased the expression of M2a cell surface markers, while M2c cells did not experience any notable changes. The proportions of M2b-subtype cells in vitro and in vivo were increased in response to GQD treatment. In summary, among M2-type cells, M2b macrophages were directly influenced and were responsible for mobilizing T_{regs} at the colon in an inflammatory milieu.

DISCUSSION

GQDs recovered intestinal immune homeostasis by suppressing excessive inflammation and facilitating the development of a regulatory loop of T cells. Intestinal macrophages, as a key regulator of immune tolerance, control gut homeostasis and protect tissues against excessive immune responses by maintaining the functionality of T_{regs} (23). Moreover, alternatively activated M2 macrophages also have critical roles in tissue repair (26). The ability of GQDs to mediate polarization of macrophages is less clear, and the current findings are controversial: While several studies have reported that graphene oxide (GO) treatment directed macrophage polarization to the M1 type in a size-dependent manner (27), others found that GO scaffolds increased the infiltration of M2-type cells (28). Using the report of Ma et al. (27) on the immunostimulatory function of GOs, we found that GQDs activate M0 cells to polarize toward the M1-type and suppress M2-type cell development. More importantly, GQDs exert potent immunosuppression in inflammatory environments in vitro and in vivo by converting M1 into M2 macrophages, which is consistent with the study of Nishida et al. (28). In line with previous reports, we also found that GQDs alleviate colitis in mice by polarizing macrophages into M2 type and resulting in an increase of T_{reg} development.

The underlying mechanism of GQDs on immunosuppression is still under research; however, we could interpret the mode of actions based on its structure. As GQDs have a conjugated graphitic domain and abundant hydrogen-donating functional groups on the edges, they are well known for their potent antioxidant effect. Because inflammation is associated with the imbalance between oxidative stress and antioxidants, GQDs' ability to scavenge reactive oxygen species (ROS) can assist in regulating inflammation. We also found that GQD treatment decreases the ROS level in THP-1 macrophages (fig. S8A). GQDs inhibited IFN-γ secretion in THP-1 cells, as we observed in primary macrophages (fig. S8B). At the same time, GQDs increased M2 marker–expressing cells, as shown by N-acetylcysteine (NAC), which is known as ROS scavenger (fig. S8C). This finding implies that GQDs regulate ROS in proinflammatory M1 macrophages, resulting in M2 polarization of macrophages.

Besides the antioxidant effect of GQDs, inflammatory cytokines such as TNF-α and IL-10, which are known to be in correlation with the ROS level, were regulated by GQDs. On the basis of the previous research, elevating the superoxide dismutase level through genetic modification could substantially ameliorate DSS-induced colitis (29). TNF-α, a proinflammatory cytokine produced from CD4$^+$ cells and M1 macrophages, is known to induce ROS generation, and the treatment of antioxidants can decrease the ROS-derived damages (30). In the presence of GQDs, the TNF-α level decreased significantly, therefore inhibiting further oxidative damage by ROS production.

In the absence of IL-10, colitis can be induced through robust intestinal inflammation (31), and research on regulating IL-10 level in IBD patients as a therapeutic target has been carried on (32). IL-10 inhibits the production of ROS from the macrophage, and by treating NAC, remarkable improvements in the DSS-induced colitis disease was observed (33). By treating GQDs, the level of IL-10 was highly elevated, showing the potential to function as a therapeutic strategy.

Another factor to consider is that GQDs have a negative surface charge due to carboxyl and hydroxyl groups. The research on the effect of nanoparticle's surface charge on inflammation and immunoregulation has been carried on, and many studies revealed that negatively charged nanoparticles are less prone to provoke immunostimulation (10). As the leading treatment target of colitis is to ameliorate excessive immune responses, injected particles must not induce additional stimulation on the immune system.

Although these findings suggest that the properties of GQDs, including the lateral size, height, and functional groups, are suitable for the use in a clinical application against colitis, it needs to be further investigated whether modifications to GQDs, such as changes to the surface charge, the ratio between functional groups, or addition of a bactericidal effect to the materials, may cause different therapeutic outcomes (34). In addition to this, various animal models, such as IL-10 knockout or CD45 T cell–transferred mice, and consequentially clinical trials can be envisioned for challenging the feasibility.

Despite the fact that GQDs were found in the abdominal cavity, when GQDs are intraperitoneally or intravenously injected, they are distributed through the whole organs and are mainly accumulated in the liver and spleen (35). In line with the previous study, we found that injected GQDs preferred to accumulate on greater omentum and mesentery near spleen and colon. Then, the particles are mostly excreted through urine or removed by hepatocytes in the liver through endocytosis (36). Also, as GQDs are composed of the hydrophobic graphitic domain and hydrophilic functional groups, and due to their small size, luminal uptake through endocytosis is probable (37). Besides the clearance of GQDs through urine, enzymes such as MPO and horseradish peroxidase are known to degrade GQDs (38). Once they are degraded and become smaller particles, it is much easier to be cleared out through the kidney, as particles smaller than 5 nm are proved to be rapidly excreted through urine (39). Therefore, GQDs could be cleared out naturally without generating noticeable toxicity. Nevertheless, validation of the therapeutic efficiency of GQDs via oral administration remains to be determined for actual therapeutic use in practice. With oral administration, the effect of GQDs can be relatively limited to a specific organ, reducing systemic side effects that appeared by any chance.

Overall, intraperitoneally injected GQDs attenuated intestinal inflammation in both acute and chronic DSS-induced experimental colitis models. GQDs effectively regulated excessive immune responses and prevented tissue damage by indirectly inducing colonic and splenic infiltration of T_{regs} and converting classical macrophages (M1) to alternative macrophages (M2), particularly the M2b subtype, in the proinflammatory milieu. With negligible toxicity and natural clearance, GQDs were able to maintain intestinal immune homeostasis, showing a potency to be used in treating IBDs.

MATERIALS AND METHODS
Preparation of GQDs
First, pristine GOs were synthesized through the improved Hummer's method (15). To prepare GQDs, the obtained solution of GOs in deionized water (3 mg/ml) was vigorously tip-sonicated for 3 hours and

vacuum-filtered with cellulose nitrate membrane filter (0.45 μm; GE Healthcare Life Science, Buckinghamshire, UK).

Biotinylation of GQDs
The biotinylation of GQDs was achieved by 1-ethyl-3-(3-dimethylaminopropyl) carbodiimide (EDC) coupling. First, 10 mg of N-(3-dimethylaminopropyl)-N′-ethylcarbodiimide hydrochloride, EDC reagent (Sigma-Aldrich, St. Louis, MO, USA), was added to 10 ml of GQD solution (3 mg/ml) to replace the edge carboxyl groups with EDC reagents. After 30 min, 20 mg of Amine-PEG$_3$-Biotin (Thermo Fisher Scientific, San Jose, CA, USA) was subsequently added to the solution to form amide bonds between activated edges of GQDs, and reactive amine groups of biotin for 24 hours. The solution was then dialyzed with a 1-kD molecular weight cut-off nitrocellulose membrane bag (Thermo Fisher Scientific, Hampton, NH, USA) to discard unreacted EDC and biotin molecules. The concentration of the final product was measured by obtaining powder after freeze-drying small amount of the solution.

TEM imaging
The sample solutions (10 μg/ml) were adsorbed to 300 mesh lacey carbon-coated copper grids (Ted Pella Inc., Redding, CA, USA) for 30 min. The grids were rinsed with a few drops of DI water and thoroughly dried in a desiccator before imaging. The samples were analyzed by a high-resolution TEM (JEM-3010, JEOL Ltd.), and the images were collected with a Gatan digital camera (MSC-794) coupled to the microscope.

Atomic force microscopy
The GQD sample was prepared on a silicon wafer and was measured by XE-100 AFM (Park Systems, Suwon, Republic of Korea) by noncontact mode. The image size of 25 μm^2 was obtained at a scan rate of 0.8 Hz.

Raman spectroscopy
The powder products were prepared on SiO$_2$ substrates for the Raman spectra measurements. The spectra were obtained with a Renishaw micro-Raman spectrometer with 514.5-nm Ar excitation laser.

FT-IR spectroscopy
Before the FT-IR spectra measurements, the powder samples were fully dried in a desiccator to prevent undesirable oxygen-containing peaks. The spectra were measured by the conventional KBr pellet method (Nicolet 6700, Thermo Fisher Scientific).

Elemental analysis
The GQD powder was obtained by freeze-drying the solution and was kept in a desiccator for more than 3 days to avoid contamination from other elements. The weight percentage of each elements was measured with an automatic elemental analyzer (FLASH 2000, Thermo Fisher Scientific).

X-ray photoelectron spectroscopy
The GQD powder was prepared by the same method as for element analysis. The binding energy of C1s was measured by XPS (AXIS-HSi, KRATOS).

Zeta potential
The GQD solution (50 μg/ml) was filtered with a 200-nm syringe filter, and the zeta potential was measured using Zetasizer Nano ZS (Malvern Instruments Ltd, Malvern, UK).

Animals
All animal experiments were carried out in accordance with the approved guidelines of Seoul National University Institutional Animal Care and Use Committee (IACUC no. SNU-170523-4). For induction of acute colitis, 6-week-old male C57BL/6 mice (Orientbio, Sungnam, Republic of Korea) were grouped randomly and given 3% DSS in drinking water for 7 days (16 mice per group). On day 1, one day after DSS induction, the mice were injected intraperitoneally with GQDs (15 mg/kg). Chronic experimental colitis was induced by repetitive administration of 3.5% DSS solution and fresh water. The body weights of the mice were measured daily, and the DAI, which is composed of body weight loss, activity, stool consistency, bleeding, and hair condition, was evaluated on day 10 for the acute model and on day 27 for the chronic model. After the mice were anesthetized, spleens, large intestines, and blood samples were collected for more ex vivo examinations.

Histopathological evaluation
Colon samples were fixed in 10% formalin for more than 24 hours and were processed following a typical method, including dehydration with ethanol, clearing with xylene, and wax infiltration with paraffin. Paraffin-embedded blocks were sectioned to 5-μm thickness and stained with hematoxylin and eosin (H&E), Masson's trichrome, and picrosirius red. Loss of goblet cells, hyperemia/edema, infiltration of immune cells, the presence of crypt abscesses, and loss of epithelium were scored on a histopathological index by H&E staining. The area of fibrotic tissue was measured by Masson's trichrome staining for the acute model and by picrosirius red for the chronic model and was quantified using ImageJ software version 1.46r (U.S. National Institutes of Health, Bethesda, MD, USA).

Cytokine detection
To determine the secretion levels of various cytokines, serum samples isolated from blood and culture supernatants of cells were prepared. To measure levels of cytokines in vivo, the Cytometric Bead Array (CBA) Kit for Mouse Inflammation (BD Biosciences, San Jose, CA, USA), the CBA flex for IL-17A and IL-23 (BD Biosciences), and enzyme-linked immunosorbent assay (ELISA) kits for MPO (R&D Systems, Minneapolis, MN, USA) and TGF-β1 (Thermo Fisher Scientific) were used according to the manufacturer's protocols. The CBA Kit for T$_H$1/T$_H$2/T$_H$17 (BD Biosciences) was used to evaluate cytokine secretion of the primary immune cell–induced specific lineages in vitro. The results were detected using flow cytometry and a spectrophotometer.

In vivo safety and toxicity evaluation of GQDs
To determine safety and possible toxicity, 300 μg of GQDs (per head, 15 mg/kg) was intraperitoneally infused and monitored for 16 weeks. The body weights and amount of intake (feed and water) per day were assessed at designated time points. After mice were sacrificed, weights of major organs were measured, and the composition of immune cells in the spleen was determined by flow cytometric analysis. To examine the level of proinflammatory cytokines, blood samples were collected, and we conducted CBA analysis according to the manufacturer's instructions.

Tracking of GQDs
For in vivo trafficking and analysis of excretion levels, biotinylated GQDs were intraperitoneally infused. To determine the remaining amounts of GQDs, mesentery tissue was collected after mice were sacrificed. After the tissue was minced and homogenized, it was incubated with FITC-conjugated anti-biotin antibody (BD Biosciences).

Fluorescence was assessed using flow cytometric analysis. In addition, urine samples were also collected at designated time points to investigate excretion as described in a previous report (*14*). The concentrations of the GQDs in urine samples were measured by the Quant*Tag Biotin Kit (Vector Laboratories Inc., Burlingame, CA, USA).

Isolation and culture of human mononuclear cells

All experimental procedures involving hUCB-derived cells were carried out in accordance with the approved guidelines of the Boramae Hospital Institutional Review Board (IRB) and the Seoul National University IRB (IRB no.1707/001-008). hUCB-mononuclear cells were isolated and cultured as previously described (*18*). Briefly, UCB samples were collected immediately after delivery with informed consent and parental approval. The UCB samples were mixed with HetaSep solution (STEMCELL Technologies, Vancouver, Canada) at a ratio of 5:1 and incubated at room temperature for 1 hour. Then, the supernatant was collected with Ficoll, and mononuclear cells were separated after centrifugation at 2500 rpm for 20 min. The cells were washed twice in PBS. Using the isolated cells, other experimental processes were conducted for further in vitro analyses.

Isolation and polarization of T cells

Naïve $CD4^+$ T cells were separated from freshly isolated hUCB-MNCs with the Human Naïve $CD4^+$ T Cell Isolation Kit II (Miltenyi Biotec, Bergisch Gladbach, Germany) according to the manufacturer's instructions. Naïve $CD4^+$ T cells were cultured in RPMI 1640 (Gibco-BRL, Grand Island, NY, USA) supplemented with 10% of fetal bovine serum (FBS), anti-CD3/28 bead activator, and IL-2 (20 ng/ml), which were essential for the proliferation of the T cell subsets. To differentiate the cells toward T cell subtypes, type-specific cytokines were added to the growth medium [IFN-γ (20 ng/ml) and IL-12 (20 ng/ml) for type 1 helper T cells and TGF-β1 (20 ng/ml) for T_{regs}], and cells were cultured for 5 days at 37°C in a humidified atmosphere with 5% CO_2 in the presence/absence of GQDs. Polarized T_H1 and T_{regs} were verified with type-specific staining and flow cytometry. For T_H1 cells, surface staining with CD4 antibody was followed by intracellular staining for IFN-γ, while CD4, CD25, and FoxP3 antibodies were used for the T_{reg} analysis.

Isolation and polarization of macrophages

Macrophages were separated from freshly isolated hUCB-MNCs with the Human $CD14^+$ Monocyte-like Cell Isolation Kit (Miltenyi Biotec, Bergisch Gladbach, Germany) according to the manufacturer's instructions. $CD14^+$ monocyte-like cells were cultured in RPMI 1640 (Gibco-BRL) supplemented with 10% FBS and stabilized for 2 days with GM-CSF (granulocyte-macrophage colony-stimulating factor) for M1 and with M-CSF (macrophage colony-stimulating factor) for M2. To polarize the cells toward macrophage subtypes, type-specific cytokines were added to the growth medium [M1: IFN-γ (20 ng/ml) and lipopolysaccharide (LPS) (1 μg/ml); M2a: IL-4 (20 ng/ml) and IL-13 (20 ng/ml); M2b: LPS (1 μg/ml), polyinosinic:polycytidylic acid (Poly I:C) (10 μg/ml), and IL-1β (20 ng/ml); M2c: IL-10 (20 ng/ml) and TGF-β1 (20 ng/ml)], and cells were cultured for 5 days at 37°C in a humidified atmosphere with 5% CO_2 in the presence/absence of GQDs. To verify the effects of graphene derivatives on the polarization of macrophages, flow cytometry and immunostaining were used. A CD14 antibody was used as an overall macrophage marker, and antibodies against CD86, CD163, and CD206 were applied as specific markers for M1 and M2 subtypes. Primary M1-polarized mac-

rophages in the presence of GQDs were subsequently cocultured with naïve $CD4^+$ T cells supplemented with the T_{reg}-specific growth factors IL-2 and TGF-β1.

Cell proliferation assay

To measure the proliferation of the cells, the Cell Proliferation ELISA Kit (Roche, Indianapolis, IN, USA) was used according to the manufacturer's instructions. The bromodeoxyuridine (BrdU) cell proliferation assay was conducted as previously described (*18*). Briefly, the cells were incubated with 100 μM of BrdU-labeling reagent for 2 hours at 37°C in a humidified atmosphere with 5% CO_2. After 30 min of fixation with the provided FixDenat solution, the cells were incubated in anti-BrdU antibody solution for 90 min and in the provided substrate (tetramethylbenzidine) solution for 5 to 30 min at room temperature. After pouring stop solution into each well, the level of cell proliferation was quantified by measuring the absorbance at wavelengths of 450 and 690 nm (as a reference).

Quantitative reverse transcription polymerase chain reaction

Total RNA was extracted using TRIzol (Invitrogen, Carlsbad, CA, USA) according to the manufacturer's instructions. The acquired RNA was used to synthesize complementary DNA (cDNA) by the SuperScript First-Strand Synthesis System (Invitrogen). The relative expression levels of target mRNAs were measured using SYBR Green PCR Master Mix (Applied Biosystems, Foster City, CA, USA) with an ABI 7300 detection system. At least three independent analyses were conducted for each gene. Detailed information for primers were described in table S2.

Cell cycle assay

Cells were fixed with ice-cold 70% ethanol at −20°C for more than 30 min. The fixed cells were washed in PBS and incubated with 400 μl of PBS containing ribonuclease A (RNase A; 7.5 μg/ml) and propidium iodide (PI) (50 μg/ml) at 37°C for 30 min. Cell cycles were analyzed by flow cytometry, which was performed on a FACSCalibur using CellQuest software (BD Biosciences).

Apoptosis assay

Cells were stained with 5 μl of FITC annexin V and 5 μl of PI using Apoptosis Detection Kits (BD Biosciences). The mixtures were gently vortexed and incubated for 15 min at room temperature in the dark. Then, 400 μl of 1× binding buffer was added to the mixtures, and all samples were analyzed by flow cytometry, which was performed on a FACSCalibur using CellQuest software (BD Biosciences).

Immunofluorescence analysis

Cells were fixed with 4% paraformaldehyde in PBS for 15 min at room temperature and were then permeabilized with 0.25% Triton X-100 (Sigma-Aldrich) for 10 min. The fixed cells were incubated with blocking solution (5% normal goat serum) for 1 hour at room temperature and incubated with primary antibodies overnight at 4°C. The cells were incubated with secondary antibodies labeled with Alexa Fluor 488 and 594 (Invitrogen). 4′,6-Diamidino-2-phenylindole (DAPI; Sigma-Aldrich) staining was conducted for 5 min to stain nuclei.

For whole-tissue immunofluorescence, the paraffin slides were deparaffinized and then blocked with PBS containing 5% normal goat serum. The sections were incubated with primary antibodies overnight. Then, the sections were incubated with Alexa Fluor 488

(Invitrogen) followed by DAPI staining. Images were captured using a confocal microscope (Eclipse TE200, Nikon, Japan).

ROS measurements

THP-1 cells were treated with 100 nM phorbol 12-myristate 13-acetate (PMA) for 24 hours and then treated with IFN-γ (20 ng/ml) and LPS (1 μg/ml) with or without GQDs for 24 hours. After washing the cells with PBS, the medium was changed to serum-free Dulbecco's modified Eagle's medium (DMEM) containing 20 μM H_2DCFDA (Invitrogen) at 37°C. Thirty minutes after the treatment, cells were washed and collected to be analyzed using flow cytometry, which was performed on a FACSCalibur using CellQuest software (BD Biosciences).

THP-1 differentiation

THP-1 cells were treated with 100 nM PMA for 24 hours and then treated with IFN-γ (20 ng/ml) and LPS (1 μg/ml) with or without GQDs for 24 hours. NAC (8 mM) was treated before the PMA treatment for 1 hour, and 1 μM H_2O_2 was treated with IFN-γ and LPS for 24 hours.

Statistical analysis

The results are expressed as means ± SD. Statistical analyses were conducted using Student's two-tailed t test or one-way analysis of variance (ANOVA) followed by the Bonferroni post hoc test for multigroup comparisons using GraphPad Prism version 8.0 (GraphPad Software, San Diego, CA, USA). Statistical significance is indicated in the figure legends.

SUPPLEMENTARY MATERIALS

Supplementary material for this article is available at http://advances.sciencemag.org/cgi/content/full/6/18/eaaz2630/DC1

View/request a protocol for this paper from *Bio-protocol*.

REFERENCES AND NOTES

1. A. Kaser, R. S. Blumberg, The road to Crohn's disease. *Science* **357**, 976–977 (2017).
2. B. Khor, A. Gardet, R. J. Xavier, Genetics and pathogenesis of inflammatory bowel disease. *Nature* **474**, 307–317 (2011).
3. G. G. Kaplan, The global burden of IBD: From 2015 to 2025. *Nat. Rev. Gastroenterol. Hepatol.* **12**, 720–727 (2015).
4. P. S. Dulai, C. A. Siegel, J.-F. Colombel, W. J. Sandborn, L. Peyrin-Biroulet, Systematic review: Monotherapy with antitumour necrosis factor α agents versus combination therapy with an immunosuppressive for IBD. *Gut* **63**, 1843–1853 (2014).
5. S. Zhang, J. Ermann, M. D. Succi, A. Zhou, M. J. Hamilton, B. Cao, J. R. Korzenik, J. N. Glickman, P. K. Vemula, L. H. Glimcher, G. Traverso, R. Langer, J. M. Karp, An inflammation-targeting hydrogel for local drug delivery in inflammatory bowel disease. *Sci. Transl. Med.* **7**, 300ra128 (2015).
6. A. Stallmach, S. Hagel, T. Bruns, Adverse effects of biologics used for treating IBD. *Best Pract. Res. Clin. Gastroenterol.* **24**, 167–182 (2010).
7. R. Caruso, T. Mathes, E. C. Martens, N. Kamada, A. Nusrat, N. Inohara, G. Núñez, A specific gene-microbe interaction drives the development of Crohn's disease–like colitis in mice. *Sci. Immunol.* **4**, eaaw4341 (2019).
8. M. J. Feito, M. Vila, M. C. Matesanz, J. Linares, G. Gonçalves, P. A. A. P. Marques, M. Vallet-Regí, J. M. Rojo, M. T. Portolés, *In vitro* evaluation of graphene oxide nanosheets on immune function. *J. Colloid Interface Sci.* **432**, 221–228 (2014).
9. V. Volarevic, V. Paunovic, Z. Markovic, B. Simovic Markovic, M. Misirkic-Marjanovic, B. Todorovic-Markovic, S. Bojic, L. Vucicevic, S. Jovanovic, N. Arsenijevic, I. Holclajtner-Antunovic, M. Milosavljevic, M. Dramicanin, T. Kravic-Stevovic, D. Ciric, M. L. Lukic, V. Trajkovic, Large graphene quantum dots alleviate immune-mediated liver damage. *ACS Nano* **8**, 12098–12109 (2014).
10. M. A. Dobrovolskaia, S. E. McNeil, Immunological properties of engineered nanomaterials. *Nat. Nanotechnol.* **2**, 469–478 (2007).
11. M. Orecchioni, C. Ménard-Moyon, L. G. Delogu, A. Bianco, Graphene and the immune system: Challenges and potentiality. *Adv. Drug Deliv. Rev.* **105**, 163–175 (2016).
12. R. Guerrero-Alba, E. E. Valdez-Morales, N. N. Jimenez-Vargas, C. Lopez-Lopez, J. Jaramillo-Polanco, T. Okamoto, Y. Nasser, N. W. Bunnett, A. E. Lomax, S. J. Vanner, Stress activates pronociceptive endogenous opioid signalling in DRG neurons during chronic colitis. *Gut* **66**, 2121–2131 (2017).
13. M. Perše, A. Cerar, Dextran sodium sulphate colitis mouse model: Traps and tricks. *J. Biomed. Biotechnol.* **2012**, 718617 (2012).
14. D. Kim, J. M. Yoo, H. Hwang, J. Lee, S. H. Lee, S. P. Yun, M. J. Park, M. Lee, S. Choi, S. H. Kwon, S. Lee, S.-H. Kwon, S. Kim, Y. J. Park, M. Kinoshita, Y.-H. Lee, S. Shin, S. R. Paik, S. J. Lee, S. Lee, B. H. Hong, H. S. Ko, Graphene quantum dots prevent α-synucleinopathy in Parkinson's disease. *Nat. Nanotechnol.* **13**, 812–818 (2018).
15. D. C. Marcano, D. V. Kosynkin, J. M. Berlin, A. Sinitskii, Z. Sun, A. Slesarev, L. B. Alemany, W. Lu, J. M. Tour, Improved synthesis of graphene oxide. *ACS Nano* **4**, 4806–4814 (2010).
16. A. C. Mullen, F. A. High, A. S. Hutchins, H. W. Lee, A. V. Villarino, D. M. Livingston, A. L. Kung, N. Cereb, T. P. Yao, S. Y. Yang, S. L. Reiner, Role of T-bet in commitment of TH1 cells before IL-12-dependent selection. *Science* **292**, 1907–1910 (2001).
17. M. C. Fantini, C. Becker, I. Tubbe, A. Nikolaev, H. A. Lehr, P. Galle, M. F. Neurath, Transforming growth factor β induced FoxP3+ regulatory T cells suppress Th1 mediated experimental colitis. *Gut* **55**, 671–680 (2006).
18. H.-S. Kim, T.-H. Shin, B.-C. Lee, K.-R. Yu, Y. Seo, S. Lee, M.-S. Seo, I.-S. Hong, S. W. Choi, K.-W. Seo, G. Núñez, J.-H. Park, K.-S. Kang, Human umbilical cord blood mesenchymal stem cells reduce colitis in mice by activating NOD2 signaling to COX2. *Gastroenterology* **145**, 1392–403e1–8 (2013).
19. T. Kobayashi, S. Okamoto, T. Hisamatsu, N. Kamada, H. Chinen, R. Saito, M. T. Kitazume, A. Nakazawa, A. Sugita, K. Koganei, K. Isobe, T. Hibi, IL23 differentially regulates the Th1/Th17 balance in ulcerative colitis and Crohn's disease. *Gut* **57**, 1682–1689 (2008).
20. L. Rovedatti, T. Kudo, P. Biancheri, M. Sarra, C. H. Knowles, D. S. Rampton, G. R. Corazza, G. Monteleone, A. Di Sabatino, T. T. MacDonald, Differential regulation of interleukin-17 and interferon-γ production in inflammatory bowel disease. *Gut* **58**, 1629–1636 (2009).
21. D. Yen, J. Cheung, H. Scheerens, F. Poulet, T. McClanahan, B. Mckenzie, M. A. Kleinschek, A. Owyang, J. Mattson, W. Blumenschein, E. Murphy, M. Sathe, D. J. Cua, R. A. Kastelein, D. Rennick, IL-23 is essential for T cell–mediated colitis and promotes inflammation via IL-17 and IL-6. *J. Clin. Invest.* **116**, 1310–1316 (2006).
22. M. Gross, T.-M. Salame, S. Jung, Guardians of the gut—Murine intestinal macrophages and dendritic cells. *Front. Immunol.* **6**, 254 (2015).
23. T. L. Denning, Y.-C. Wang, S. R. Patel, I. R. Williams, B. Pulendran, Lamina propria macrophages and dendritic cells differentially induce regulatory and interleukin 17-producing T cell responses. *Nat. Immunol.* **8**, 1086–1094 (2007).
24. A. Mantovani, A. Sica, S. Sozzani, P. Allavena, A. Vecchi, M. Locati, The chemokine system in diverse forms of macrophage activation and polarization. *Trends Immunol.* **25**, 677–686 (2004).
25. W. Zhang, W. Xu, S. Xiong, Blockade of Notch1 signaling alleviates murine lupus via blunting macrophage activation and M2b polarization. *J. Immunol.* **184**, 6465–6478 (2010).
26. F. O. Martinez, S. Gordon, The M1 and M2 paradigm of macrophage activation: Time for reassessment. *F1000Prime Rep.* **6**, 13 (2014).
27. J. Ma, R. Liu, X. Wang, Q. Liu, Y. Chen, R. P. Valle, Y. Y. Zuo, T. Xia, S. Liu, Crucial role of lateral size for graphene oxide in activating macrophages and stimulating pro-inflammatory responses in cells and animals. *ACS Nano* **9**, 10498–10515 (2015).
28. E. Nishida, H. Miyaji, A. Kato, H. Takita, T. Iwanaga, T. Momose, K. Ogawa, S. Murakami, T. Sugaya, M. Kawanami, Graphene oxide scaffold accelerates cellular proliferative response and alveolar bone healing of tooth extraction socket. *Int. J. Nanomed.* **11**, 2265–2277 (2016).
29. A. Roessner, D. Kuester, P. Malfertheiner, R. Schneider-Stock, Oxidative stress in ulcerative colitis-associated carcinogenesis. *Pathol. Res. Pract.* **204**, 511–524 (2008).
30. B. Yan, H. Wang, Z. N. Rabbani, Y. Zhao, W. Li, Y. Yuan, F. Li, M. W. Dewhirst, C.-Y. Li, Tumor necrosis factor-α is a potent endogenous mutagen that promotes cellular transformation. *Cancer Res.* **66**, 11565–11570 (2006).
31. W. K. E. Ip, N. Hoshi, D. S. Shouval, S. Snapper, R. Medzhitov, Anti-inflammatory effect of IL-10 mediated by metabolic reprogramming of macrophages. *Science* **356**, 513–519 (2017).
32. M.-C. Li, S.-H. He, IL-10 and its related cytokines for treatment of inflammatory bowel disease. *World J. Gastroenterol.* **10**, 620–625 (2004).
33. B. Li, R. Alli, P. Vogel, T. L. Geiger, IL-10 modulates DSS-induced colitis through a macrophage–ROS–NO axis. *Mucosal Immunol.* **7**, 869–878 (2014).
34. S. Liu, T. H. Zeng, M. Hofmann, E. Burcombe, J. Wei, R. Jiang, J. Kong, Y. Chen, Antibacterial activity of graphite, graphite oxide, graphene oxide, and reduced graphene oxide: Membrane and oxidative stress. *ACS Nano* **5**, 6971–6980 (2011).
35. N. Lu, N. Wang, M. Lv, Z. Tang, C. Fan, Graphene-based nanomaterials in biosystems. *Nano Res.* **12**, 247–264 (2019).
36. K. Yang, J. Wan, S. Zhang, Y. Zhang, S.-T. Lee, Z. Liu, *In vivo* pharmacokinetics, long-term biodistribution, and toxicology of PEGylated graphene in mice. *ACS Nano* **5**, 516–522 (2011).

37. H. Zhang, C. Peng, J. Yang, M. Lv, R. Liu, D. He, C. Fan, Q. Huang, Uniform ultrasmall graphene oxide nanosheets with low cytotoxicity and high cellular uptake. *ACS Appl. Mater. Interfaces* **5**, 1761–1767 (2013).

38. R. Kurapati, J. Russier, M. A. Squillaci, E. Treossi, C. Ménard-Moyon, A. E. Del Rio-Castillo, E. Vazquez, P. Samorì, V. Palermo, A. Bianco, Dispersibility-dependent biodegradation of graphene oxide by myeloperoxidase. *Small* **11**, 3985–3994 (2015).

39. M. Nurunnabi, Z. Khatun, K. M. Huh, S. Y. Park, D. Y. Lee, K. J. Cho, Y.-K. Lee, In vivo biodistribution and toxicology of carboxylated graphene quantum dots. *ACS Nano* **7**, 6858–6867 (2013).

Citation: B.-C. Lee, J. Y. Lee, J. Kim, J. M. Yoo, I. Kang, J.-J. Kim, N. Shin, D. J. Kim, S. W. Choi, D. Kim, B. H. Hong, K.-S. Kang, Graphene quantum dots as anti-inflammatory therapy for colitis. *Sci. Adv.* **6**, eaaz2630 (2020).

Science Advances

Graphene quantum dots as anti-inflammatory therapy for colitis

Byung-Chul Lee, Jin Young Lee, Juhee Kim, Je Min Yoo, Insung Kang, Jae-Jun Kim, Nari Shin, Dong Jin Kim, Soon Won Choi, Donghoon Kim, Byung Hee Hong and Kyung-Sun Kang

ARTICLE TOOLS	http://advances.sciencemag.org/content/6/18/eaaz2630
SUPPLEMENTARY MATERIALS	http://advances.sciencemag.org/content/suppl/2020/04/27/6.18.eaaz2630.DC1
REFERENCES	This article cites 39 articles, 12 of which you can access for free http://advances.sciencemag.org/content/6/18/eaaz2630#BIBL
PERMISSIONS	http://www.sciencemag.org/help/reprints-and-permissions